Journal of The Electrochemical Society, **150** (10) H229-H234 (2003) H229
0013-4651/2003/150(10)/H229/6/$7.00 © The Electrochemical Society, Inc.

Simultaneous AFM and QCM Measurements

Methodology Validation Using Electrodeposition

J.-M. Friedt,[z] K. H. Choi, F. Frederix, and A. Campitelli

IMEC, 3001 Leuven, Belgium

We assess the validity and advantages of using a quartz crystal microbalance (QCM) as the metallic-coated substrate used for atomic force microscopy (AFM) measurements by studying two well-known electrochemical reactions, silver electrodeposition on gold and copper electrodeposition on gold. We compare the results provided by electrochemistry (cyclic voltammetry), QCM frequency, and damping variations as well as AFM topography, and analyze the advantages of combining the three methods in the same instrument. Comparison of the evolution of the frequency of the third and fifth QCM overtones allows identification of the type of interaction between the sensing electrode and its environment: a rigid layer when the frequency shift is proportional to the overtone number, viscous interaction when the frequency shift is proportional to the square root of the overtone number. This identification scheme leads to results confirmed by the QCM damping.
 [DOI: 10.1149/1.1603255]

Manuscript submitted October 1, 2002; revised manuscript received April 28, 2003. Available electronically August 14, 2003.

The quartz crystal microbalance (QCM) is a sensitive technique commonly used for detecting minute mass changes. It is based on an oscillating quartz plate whose resonance frequency varies with the mass adsorbed on the surface of one of the electrodes. It has been used for monitoring electrochemical reactions in a setup simultaneously using the sensing electrode of the QCM as the working electrode (WE) of the electrochemical setup.[1-3]

Scanning probe microscopy has been used more recently for monitoring electrodeposition reactions. Electrodeposition of a wide variety of metals including copper and silver has thus been observed with atomic resolution using a scanning tunneling microscope (STM).[4,5]

We have combined in the same instrument a QCM and an atomic force microscope (AFM). We use this experimental setup to simultaneously measure the mass deposited on the sensing electrode of the QCM (as observed by a shift of the resonance frequency of the crystal) and the topography of the added layer.[6] In this article we are interested in the morphology of electrodeposited films of silver or copper on gold, and their effect on the sensing mechanism of the QCM. We describe the data analysis procedure leading to a distinction of the type of interaction sensed by the QCM, *i.e.*, rigid layer or viscous layer properties, from the evolution of the frequency of the overtones of the resonator as well as the monitoring of the dissipation (being defined as the inverse of the quality factor) of the QCM. Thus, simultaneous analysis of the evolution of the frequency of the overtones and damping combined with topography analysis brings complementary information on the interactions of the QCM with its environment, and confirms a previous hypothesis of the discrepancy between predicted and observed mass sensitivities of the quartz crystal resonator,[7,8] namely the major contribution of the interaction with the surrounding viscous liquid and the inadequacy of a rigid-bound-mass model for estimating the amount of material interacting with the surface of the QCM. Identifying the conditions in which different kinds of interactions exist is necessary for applying accurate models when relating a QCM frequency shift to a deposited mass in a liquid medium.

Experimental

We have previously described the interaction of a QCM used as an active substrate for AFM measurements,[6] and shown that these two instruments only interact in a limited way which does not degrade the quality of the measurements. The vibration amplitude of the QCM is below the resolution of the AFM; the maximum in-plane displacement of a quartz resonator with a quality factor of 3000 to which a 0.5 V amplitude signal is applied at resonance frequency is predicted to be at most 3 nm. That is below the AFM lateral resolution presented in the current experiments. The moving AFM cantilever holder disturbs the resonance frequency by varying the boundary conditions of longitudinal acoustic waves generated by the QCM, but does not prevent measurement of the very large frequency shifts observed during electrodeposition, especially when monitoring the higher order overtones which are less affected.

Here we have added to the liquid cell the three electrodes required for electrochemistry, *i.e.*, the QCM sensing surface is also used as the working electrode (WE), a 0.25 mm diam platinum wire shaped in three-quarters of a circle is used as a counter electrode (CE) while a wire made of the same metal as the one to be deposited on the WE is used as the pseudo-reference electrode (RE). The sensing surface of the QCM can be simultaneously used as the electrochemical WE because the frequencies of the electrical signals generated by the two techniques widely differ; electrochemistry sweeps voltages at very low frequency (2 to 50 mV/s) while the QCM oscillates at high frequency (4.7 MHz). Hence, a simple passive inductor-capacitor (LC) network is enough to decouple the two signals and make independent measurements on the same surface[9] (Fig. 1).

The AFM was provided by Molecular Imaging (Phoenix, AZ, USA) and was operated in the tapping mode (silicon cantilever with stiffness constants in the 1.2 to 3.5 N/m range as given by the manufacturer; resonance frequency of the cantilever around 30 kHz in water; scan rate, 0.45 lines/s = 2.245 μm/s for 5 μm wide images), while the QCM parameters were measured using the electronics provided by Q-Sense AB (Göteborg, Sweden). During an experiment we acquired the frequency of the third and fifth overtones of the QCM (since we have observed and previously justified[6] that the first mode is highly unstable due to interactions with the environment) as well as the damping D ($D = 1/Q$, Q being the quality factor of the resonance) of these two modes.[10] The 14 mm diam plano-plano QCM AT-cut crystals were bought blank from Chintele Quartz Technology Co. Ltd. (Zhejiang, China), and Ti/Au (5/50 nm, respectively) electrodes were evaporated using a mechanical mask. The sensing electrode is a 12 mm diam disk which covers one surface, while the opposite surface is patterned with a key-hole-shaped electrode made of a central 5-mm diam disk and a 3 mm long, 1 mm wide lead to the edge of the crystal. The peak-to-peak roughness of the electrodes, as measured by AFM, is 3 to 5 nm. The PC3-300 potentiostat used for cyclic voltammetry was provided by Gamry Instruments (Warminster, PA, USA).

Two electrodeposition reactions were studied, copper electrodeposition on gold[4] and silver electrodeposition on gold. The 48 nm thick gold working electrode was evaporated on AT-cut quartz crystals previously cleaned in a piranha solution (proportions 3 to 7 of 96% H_2SO_4 and 30% H_2O_2, respectively) and coated with an evaporated 2 nm thick Ti adhesion layer. The platinum CE wire and the silver or copper RE wires were bought from Goodfellow (Hunt-

[z] E-mail: friedtj@imec.be

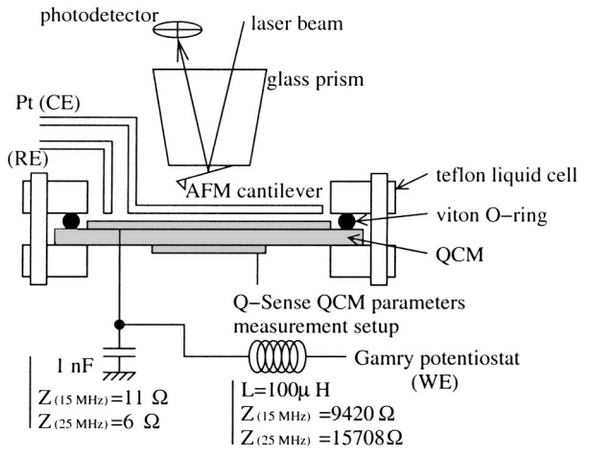

Figure 1. Experimental setup combining AFM, QCM, and electrochemistry in the same instrument. The impedance calculations are displayed to illustrate the decoupling of the high- and low-frequency signals.

ingdon, U.K.) and are specified, respectively, 99.99% pure (0.25 mm diam, annealed), 99.99% (0.125 mm diam, annealed) and 99.98^{+}% (1 mm diam, as drawn). The electrolyte solution for copper electrodeposition was made of 10^{-2} M sulfuric acid and 10 mM copper sulfate. The electrolyte solution for silver electrodeposition was made of 10 mM $AgNO_3$, 0.5 M KNO_3, and 0.1 M HNO_3. The copper wire used as the RE for the copper electrodeposition experiment was 1 mm diam, cleaned in 70% nitric acid by dipping for 5 s and kept in the solution used for the experiment for to a few days. The RE for silver electrodeposition was a 0.125 mm diam wire.

Results

We have simultaneously recorded the voltage and current applied by the potentiostat during cyclic voltammetry (Fig. 2), the frequencies (Fig. 3 and 4, Δf_3 and Δf_5 curves) and damping of the QCM (Fig. 3 and 4, ΔD_3 and ΔD_5 curves) for the third and fifth overtones as well as the topography of the sample on 5 × 5 μm (Fig. 3 and 4, top) and 2 × 2 μm (data not shown) areas. The horizontal axis of all graphs are a common time scale (graduated in seconds), while the slow scan direction (0.3 line/s) of the AFM images also extends along the horizontal axis, effectively displaying the time evolution of the surface topography. The vertical axis of the AFM images provide a snapshot of the topography during the electrodeposition processes, with 256 pixels recorded in 3 s (Fig. 5), which we assume to be isotropic and expandable in all in-plane directions.

We clearly observe the formation of copper or silver crystals on the underlying evaporated gold granular structure (initial roughness, 5 nm peak to peak). The formation of crystals during the electrodeposition step can be seen to be synchronous with the potentiostat applied potential (second curve from bottom in Fig. 3 and 4) becoming negative since the reference electrode is made of the same metal as the one deposited. The QCM frequency shift (fourth and sixth curves from bottom in Fig. 3 and 4) simultaneously provides an estimate of the total mass of metal deposited on the whole sensing electrode while the QCM dissipation (third and fifth curves from bottom in Fig. 3 and 4) increases when viscous interaction with the surrounding liquid increases.

We now compare the estimated mass of metal deposited on the QCM sensing electrode from the total charges transferred as measured by cyclic voltammetry, frequency shift from the QCM, and topography from the AFM. The number of charges transferred to the system by the electrochemical setup is numerically integrated and leads to a deposited mass of

$$M_{\text{deposited}} = \frac{M_{\text{metal}} \Sigma_j I_j \times \delta t}{Z_{\text{ion}} F} \qquad [1]$$

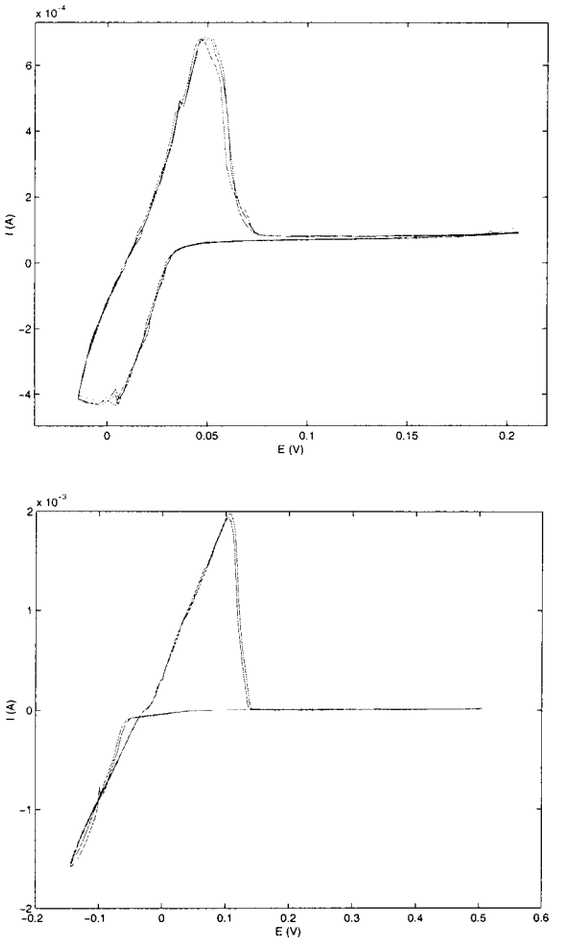

Figure 2. Top: cyclic voltametry monitored during silver electrodeposition on gold (sweep rate, 2 mV/s). Bottom: cyclic voltametry monitored during copper electrodeposition on gold (sweep rate, 5 mV/s). These figures show that even though only a pseudo-reference electrode was used, the electrodeposition cycles displayed good reproducibility.

where F is the Faraday constant ($F = N \cdot e = 96{,}440$ C, where N is the Avogadro number and e the charge of the electron), $\Sigma_j I_j$ the numerical integration of the current observed on the peak analyzed, δt the time interval between two current measurements, Z_{ion} the valence of the metallic ion (1 for silver and 2 for copper), $M_{\text{deposited}}$ the mass of metal deposited on the WE and M_{metal} the molar weight of the metal deposited on the surface (63.5 g/mol for copper and 108 g/mol for silver).

The mass sensitivity of the QCM is given by the Sauerbrey equation applied to the nth overtone (the $1/n$ factor being due to the fact that we consider the additional layer thickness in terms of wavelengths, and the wavelength of the nth overtone is $1/n$ of the fundamental wavelength)[11]

$$\Delta f_n = \frac{-2 f_n^2}{n \times A\sqrt{\rho\mu}} \Delta m = \frac{-n \times 2 f_1^2}{A\sqrt{\rho\mu}} \Delta m \qquad [2]$$

where $\rho = 2.684$ g cm^{-3} is the density of quartz, $\mu = 2.947 \times 10^{11}$ g cm^{-1} s^{-2} is the shear modulus of AT-cut quartz, A is the macroscopic sensing area taken to be 1 cm^2 on our design, f_n being the frequency $n \times 4.7$ MHz of the nth overtone (the fundamental resonance frequency being $f_1 = 4.7$ MHz). We thus deduce the mass deposited on the QCM by multiplying the normalized $\Delta f_n/n$ observed frequency shift of the nth overtone by the proportionality

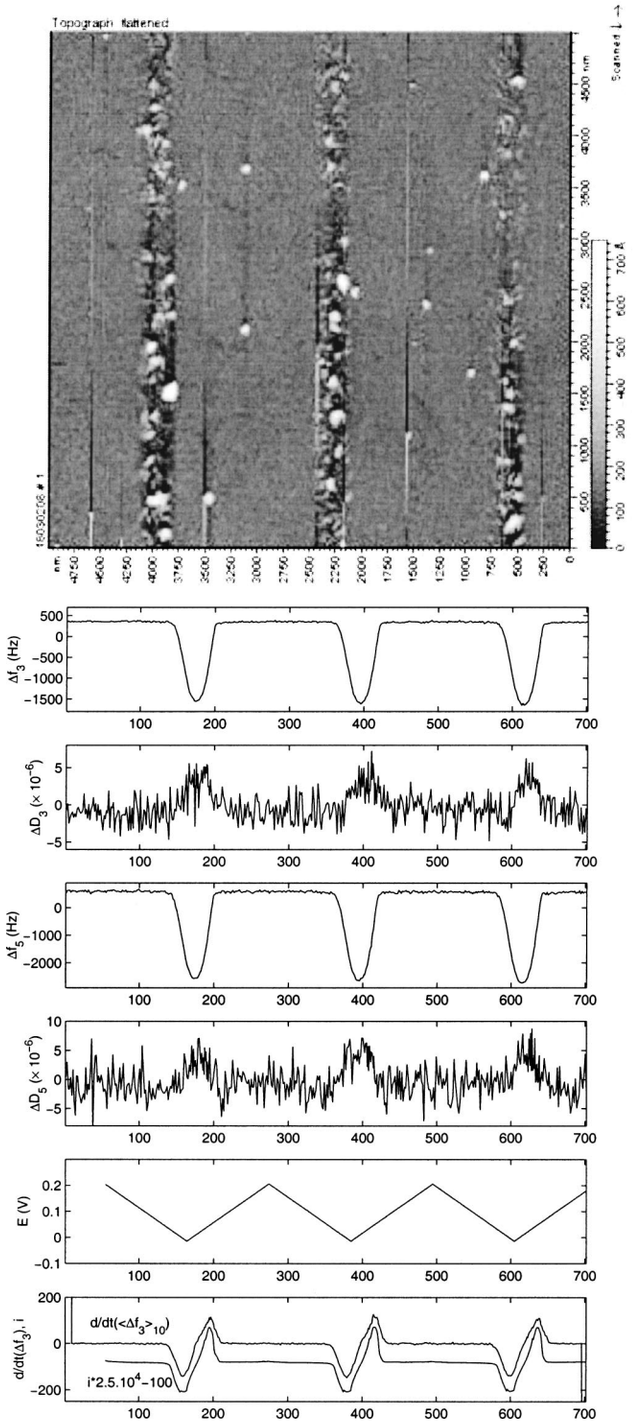

Figure 3. Top: AFM topographic image (top) obtained on a 5 × 5 μm area during silver electrodeposition. Time increases from left to right and is synchronous for all graphs. Top: the horizontal axis of the AFM topography image is the slow scan direction (0.3 line/s), while the vertical axis is the fast scan direction (256 pixels/line), providing a snapshot of the surface during the electrodeposition process. Bottom: evolution of the frequency and damping of the third and fifth overtones during silver electrodeposition, as well as voltage sweep and comparison of the current and time derivative of the frequency (which, as expected from Eq. 1, must be proportional). For the last curve, the third-mode frequency measurements were averaged over 10 samples and the current, in amperes, was multiplied by 10^4 and offset by 100 in order to be on the same scale. The multiplication factor is in agreement with the theoretical value deduced from Eq. 1, considering that the time interval between two frequency measurements is 1.52 s.

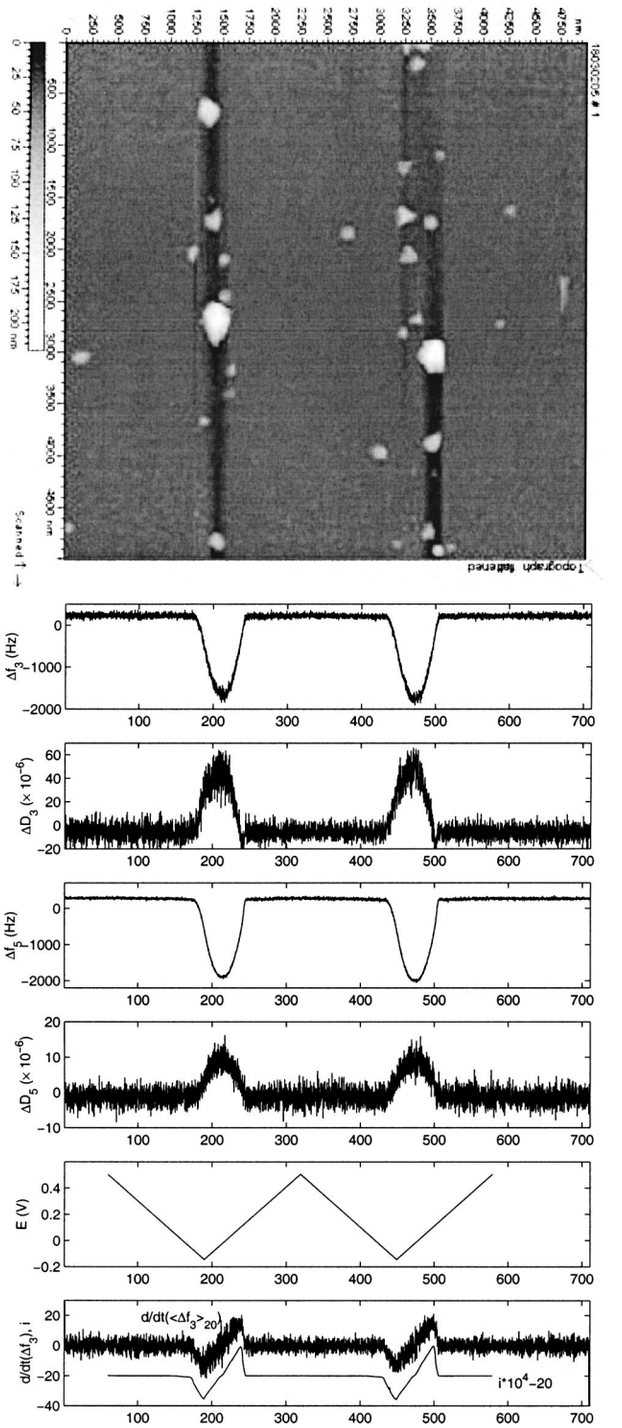

Figure 4. Top: AFM topographic image (bottom) obtained on a 5 × 5 μm area during copper electrodeposition. Time increases from left to right and is synchronous for all graphs. Top: the horizontal axis of the AFM topography image is the slow scan direction (0.3 line/s), while the vertical axis is the fast scan direction (256 pixels/line), providing a snapshot of the surface during the electrodeposition process. Bottom: evolution of the frequency and damping of the third and fifth overtones during copper electrodeposition, as well as voltage sweep and comparison of the current and time derivative of the frequency (which, as expected from Eq. 1, must be proportional). For the last curve, the third-mode frequency measurements were averaged over 20 samples and the current, in amperes, was multiplied by 2.5 × 10^4 and offset by 20 in order to be on the same scale. The multiplication factor is in agreement with the theoretical value deduced from Eq. 1, considering that the time interval between two frequency measurements is 0.14 s.

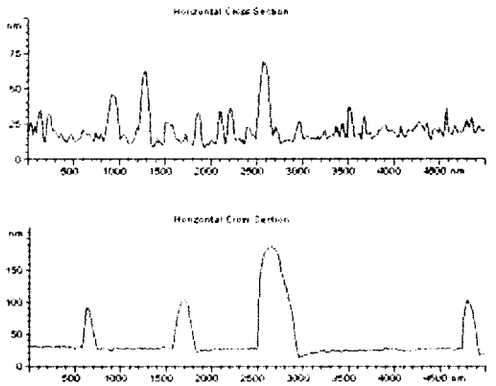

Figure 5. Cross sections of the AFM topography images at the maximum height of silver electrodeposition (top) and copper electrodeposition (bottom). Notice the vertical scale changes which display large surface roughness differences.

factor 20.1 ng/Hz. Assuming (Eq. 2) that the frequency shift of the QCM is proportional to the deposited mass, we can see here (Eq. 1) that the time derivative of the resonance frequency must be proportional to the current flowing in the potentiostat. This fact is illustrated by plotting in Fig. 3 and 4 (bottom curves) both the current and the averaged time derivative of the frequency, which indeed display very similar trends.

The volume of the metal grains deposited on the WE is estimated from the AFM topography images, using a cross section of the image at maximum crystal height as shown in Fig. 5. We assume the deposited metal layer to be uniform over the whole sensing electrode and the metal density to be equal to its tabulated bulk value (8.920 g/cm^3 for copper and 10.490 g/cm^3 for silver).

The application to our experiments of these calculations is summarized in Table I for the copper electrodeposition experiments and Table II for the silver electrodeposition experiments. Table II shows that for silver electrodeposition, the frequency shift is proportional to the overtone number, as expected from the rigid-mass approximation. By applying the Sauerbrey model, we deduce a deposited mass only marginally greater than that obtained from the number of charges flowing through the potentiostat. Supporting evidence of the validity of the rigid-mass model during silver deposition is the small variation of the QCM dissipation, which is confirmed by the flat topography provided by the AFM images (Fig. 4). On the contrary, Table I shows that the frequency shift of the QCM is not proportional to the overtone number while the dissipation of the QCM is much greater during copper electrodeposition than during silver electrodeposition. Later, we justify (Eq. 3) the relationship of the frequency overtone with the square root of the overtone number as being an indicator of a viscous interaction between the sensing electrode and the liquid medium. This conclusion is supported by the rough surface shown by AFM images during copper crystal formation (Fig. 3).

Table I. Top: numerically integrated charge transfer for the positive and negative peaks, and derived deposited mass in both cases (CV: cyclic voltammetry). Middle: QCM frequency shift and derived deposited mass from both overtone measurements. The mass derived from a rigid layer hypothesis (proportionality between the deposited mass and the frequency shift at an overtone divided by this overtone number) is displayed for comparison to Table II. Notice the large difference between the predicted masses for both overtones and compared to the CV data, leading to the inadequacy of the hypothesis. Bottom: average metallic layer thickness derived from the calculated deposited masses (from CV measurements), and comparison of the grain height (from AFM topography measurements) with QCM damping measurements.

	Cu, cycle 1	Cu, cycle 2
Negative peak	−33.4 mC	−34.8 mC
Positive peak	31.1 mC	33.0 mC
Mass CV (ng, −/+)	10996/10239	11457/10864
$\Delta f_3/\sqrt{3}$	1072 Hz	1154 Hz
$\Delta f_5/\sqrt{5}$	962 Hz	1011 Hz
Mass QCM (ng, $\Delta f_n/n$, n = 3, 5)	12440, 8647	13392, 9088
Average thickness	11.9 nm (CV)	12.5 nm (CV)
Max. peak height	160 nm	180 nm
Damping (QCM, D_3)	51×10^{-6}	51×10^{-6}

Furthermore, underpotential copper deposition (UPD) provides a means of calibrating the mass sensitivity of the QCM by replacing in the expression of the frequency shift (Eq. 2) the macroscopic geometric area A of the QCM electrodes by the sensing area at the microscopic level. We observe (Fig. 6) during voltage sweeps for copper electrodeposition the UPD region as a slow decrease in frequency due to the deposition of a single layer of copper atoms on the gold surface.[2,3,12,13] The frequency shift is observed to be 25 Hz for the third overtone and 40 Hz for the fifth overtone (Fig. 6). These two values normalize well with the overtone number, $\Delta f_3/3 = \Delta f_5/5 = 8$ Hz (within uncertainties in frequency measurements). Hence, the Sauerbrey model of the rigid adsorbed layer can be used in this case. If we consider a hexagonal dense packing of copper atoms separated by $0.362/\sqrt{2} = 0.26$ nm,[14] we obtain an atomic density of 1.175×10^{15} atom/cm^2 which thus weigh 124 ng cm^{-2}. The 8 Hz normalized frequency shift leads to a mass variation of 160.8 ng. Applying the Sauerbrey relationship with the theoretical sensitivity of the 4.7 MHz QCM and the observed frequency shift, the theoretical deposited mass of 124 ng on the 1 cm^2 working electrode can only be justified if the area at the microscopic level of 1.3 cm^2. The difference with the expected 1 cm^2 of the macroscopic geometrical dimensions of the electrodes is most certainly due to the roughness of the gold sensing electrode. This calculation assumes a

Table II. Top: numerically integrated charge transfer for the positive and negative peaks (leakage current: 80 μA, compensated for numerically during current integration by subtracting 30 μA from the readings), and derived deposited mass in both cases (CV: cyclic voltammetry). Middle: QCM frequency shift and derived deposited mass from both overtone measurements. Bottom: average metallic layer thickness derived from the calculated deposited mass (from QCM measurements), and comparison of the grain height (from AFM topography measurements) with QCM damping measurements.

	Ag, cycle 1	Ag, cycle 2	Ag, cycle 3
Negative peak	−9.8 mC	−10.1 mC	−9.8 mC
Positive peak	10.0 mC	10.4 mC	10.2 mC
Mass CV (ng, −/+)	10974/11198	11311/11647	10975/11423
$\Delta f_3/3$	631 Hz	648 Hz	660 Hz
$\Delta f_5/5$	630 Hz	635 Hz	651 Hz
Mass QCM (ng, 3/5)	12613/12596	12960/12688	13193/13020
Average thickness	12.0 nm (QCM)	12.2 nm (QCM)	12.5 nm (QCM)
Max. peak height	60 nm	55 nm	65 nm
Damping (QCM, D_3)	5×10^{-6}	5×10^{-6}	5×10^{-6}

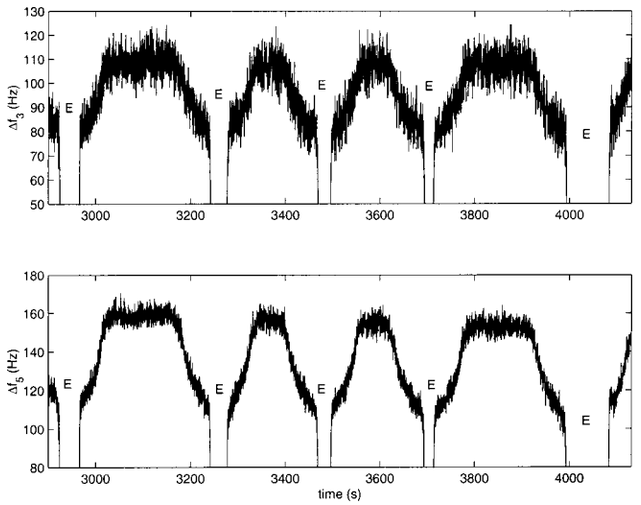

Figure 6. Englargement of expanded view on the frequency shift showing underpotential deposition of copper on gold, third overtone (top) and fifth overtone (bottom). Areas marked E are the times during which copper was electrodeposited and the frequency dropped by several hundreds of Hertz, out of range of these graphs.

denser packing of copper atoms, deduced from bulk properties, than those observed by scanning tunneling microscopy (STM) by Magnussen *et al.*[2] during electrodeposition, which would lead, if used here, to an even greater difference between the macroscopic and microscopic areas.

Discussion

When analyzing the AFM images, we must hypothesize that the reaction is occurring in the same way over the whole electrode area. This hypothesis is difficult to verify under the current experimental conditions, since the CE must be much smaller than the WE in order to leave space for the AFM cantilever holder.

We found it interesting to compare the large difference in shape and heights of the copper and silver crystals, and to analyze the damping of the QCM in this aspect. The copper electrodeposition shows very localized high crystals (80 to 120 nm in our AFM images) while the underlying gold granular structure is still visible. On the other hand, silver electrodeposition shows a much smoother surface (silver grain height ranging from 10 to 60 nm) with a total coverage of the surface. These topographic observations are well correlated with the damping measurements; the damping observed during copper electrodeposition is over ten times (from $\Delta D_3 = 5 \times 10^{-6}$ for silver electrodeposition to $\Delta D_3 = 60 \times 10^{-6}$ for copper electrodeposition) that observed during silver electrodeposition. Hence, QCM damping can be used as an indicator of the final surface smoothness.

As seen in the quantitative analysis in Tables I and II, the frequency shift that is predicted from the electrochemical charges is systematically smaller than the experimentally observed QCM frequency shift, assuming a rigid mass model. Similar, but much larger, discrepancies were reported previously.[15] This means that the sensitivity of the QCM as calculated from the Sauerbrey equation is underestimated. All parameters of the Sauerbrey formula are well characterized parameters of the material the QCM is made of (AT-cut quartz) except for the sensing area. We used the macroscopic area of 1 cm^2 while we believe the effective sensing area must be larger and actually account for the 20 to 50% discrepancy between predicted and observed frequency shift. This increase in the effective sensing mass is attributed to poor acoustic energy confinement because of the very thin, 2 nm Ti and 48 nm Au, electrodes deposited on our QCMs which lead to leakages of the acoustic field away from the actual electrode boundaries[16] and the underestimation of the actual sensing area on the microscopic level which was shown by UPD measurements to be greater than the macroscopic geometrical area (Fig. 6).

Furthermore, we notice that the frequency shifts of the overtones do not normalize well ($\Delta f_3/3 \neq \Delta f_5/5$) for the copper measurements, while the normalization leads to satisfactory results for the silver measurements. We attribute this discrepancy to the inadequacy of the Sauerbrey model for the copper layer. The hypothesis behind the Sauerbrey calculation is that the deposited layer has properties very similar to quartz (and hence only acts as an increased thickness of the resonator), and it does not interact with the surrounding liquid. Copper deposition leads to a large increase in the damping of the QCM oscillation and we thus have to conclude that the layer greatly interacts with the surrounding liquid (the water-based solution in our case). We now assume that a liquid layer of thickness δ moves with the QCM surface and adds its mass to that of the resonator. δ is for a Newtonian fluid

$$\delta = \sqrt{\frac{\eta_l}{\pi f_n \rho_l}} \qquad [3]$$

where η_l and ρ_l are, respectively, the dynamic viscosity and density of the liquid (for water, these constants are numerically equal to 0.01 g cm^{-1} s^{-1} and 1 g cm^{-3}), f_n being the resonance frequency of the nth overtone. By using a model based primarily on an interaction with the surrounding liquid,[17] we obtain a proportionality relationship between $f_n/\sqrt{n}$ and the added mass (instead of f_n/n), including the interacting liquid layer. This relationship is obtained by replacing the added thickness $\Delta m/A$ of the rigid layer used in the Sauerbrey assumptions by δ which introduces a $1/\sqrt{n}$ factor in Eq. 2 (which reflects the fact that the thickness of the water layer moved by the QCM vibration is dependent on the frequency, as opposed to a strongly bound rigid layer whose mass is constant).[18]

We indeed see from the experimental data (Tables I and II) that a scaling by $f_n/\sqrt{n}$ instead of f_n/n leads to compatible results of the third and fifth overtones. Hence, in the case of the rough copper surfaces, interaction with the surrounding liquid is a predominant effect and the mass deduced from the QCM frequency shift is not accurate since it includes the mass of liquid displaced. Notice that for oscillating frequencies of 14.1 and 23.5 MHz, δ is, respectively, 150 and 116 nm. We interpret this dependency with $1/\sqrt{n}$ of the copper deposition as an increase of the liquid layer thickness interacting with the QCM due to increased electrode surface roughness after electrodeposition.

A much more complex model, including surface roughness height and correlation length, has been developed for the fundamental oscillation mode of the QCM by Daikhin *et al.*[19-23] This model, unlike the one presented here which simply compares the penetration depth of the shear acoustic wave in the liquid with the surface roughness, is, however, difficult to extend to overtones.

Conclusions

In this experiment we have displayed the results of monitoring an electrodeposition reaction of a metal on a gold electrode simultaneously using QCM, cyclic voltammetry, and AFM. We show the complementary information brought by these three techniques and the good correlation of these results. QCM dissipation measured on the third overtone is most sensitive and well related to surface roughness as estimated from AFM topography. QCM frequency shifts are compatible with the estimated metal mass deposited on the working electrode estimated from total charge transferred measured by cyclic voltammetry.

During data analysis, we have shown how the evolution of the frequency shift with overtone numbers allows identification of the cause of the frequency shift (added mass as a rigid layer or interaction with a variable thickness of a viscous fluid), and these results match well the observed energy losses as monitored by QCM damping. Silver electrodeposition, leading to a quite smooth surface dis-

playing low damping, shows a frequency shift varying as $1/n$, n being the overtone number, as predicted by theory for a layer rigidly bound to the QCM electrode, following the Sauerbrey model. Copper electrodeposition, leading to a rougher surface displaying high damping, shows a frequency shift varying as $1/\sqrt{n}$, as predicted by theory for a viscous layer interacting with the QCM vibrating electrode. These observations mean that the QCM frequency shift during copper electrodeposition cannot be solely attributed to the mass of metal deposited on the surface, but a more refined model including viscous interaction with the surrounding liquid must be used.

An extension of the model developed by Daikhin *et al.* for the fundamental oscillation mode to the overtones of the QCM is necessary to produce a full image of the interaction of the acoustic wave with the liquid as a function of surface roughness properties.

Acknowledgments

We would like to extend our thanks to Professor L. Heerman of K. U. Leuven, Belgium, for his valuable comments on our present study.

IMEC assisted in meeting the publication costs of this article.

References

1. M. J. Henderson, E. Bitziou, A. R. Hillman, and E. Vieil, *J. Electrochem. Soc.*, **148**, E105 (2001).
2. O. M. Magnussen, J. Hotlos, R. J. Nichols, D. M. Kolb, and R. J. Behm, *Phys. Rev. Lett.*, **64**, 2929 (1990).
3. O. Melroy, K. Kanazawa, J. G. Gordon II, and D. Buttry, *Langmuir*, **2**, 697 (1986).
4. D. M. Kolb and M. A. Schneeweiss, *Electrochem. Soc. Interface*, **8**(1), 26 (1999).
5. O. M. Magnussen, J. Hotlos, G. Beitel, D. M. Kolb, and R. J. Behm, *J. Vac. Sci. Technol. B*, **9**, 969 (1991).
6. J.-M. Friedt, K. H. Choi, L. Francis, and A. Campitelli, *Jpn. J. Appl. Phys., Part 1*, **41**, 3974 (2002).
7. R. Schumacher, G. Borges, and K. K. Kanazawa, *Surf. Sci.*, **163**, L621 (1985).
8. R. Schumacher, J. G. Gordon, and O. Melroy, *J. Electroanal. Chem. Interfacial Electrochem.*, **216**, 127 (1987).
9. A. Bund and G. Schwitzgebel, *Electrochim. Acta*, **45**, 3703 (2000).
10. M. Rodahl and B. Kasemo, *Sens. Actuators A* , **54**, 448 (1996).
11. M. D. Ward and D. A. Buttry, *Science*, **249**, 1000 (1990).
12. D. A. Buttry and M. D. Ward, *Chem. Rev. (Washington, D.C.)*, **92**, 1355 (1992).
13. C. Chen and A. A. Gewirth, *Phys. Rev. Lett.*, **68**, 1571 (1992).
14. J. P. Mercier, G. Zambelli, and W. Kurz, *Introduction à la Science des Matériaux*, p. 89, Presses polytechniques et universitaires romandes, Lausanne (1999) [in French].
15. R. Schumacher, G. Borges, and K. K. Kanazawa, *Surf. Sci.*, **163**, L621 (1985).
16. A. Janshoff, H.-J. Galla, and C. Steinem, *Angew. Chem., Int. Ed. Engl.*, **39**, 4004 (2000).
17. R. Schumacher, *Angew. Chem., Int. Ed. Engl.*, **29**, 329 (1990).
18. C. M. Flanigan, M. Desai, and K. R. Shull, *Langmuir*, **16**, 9825 (2001).
19. M. Urbakh and L. Daikhin, *Phys. Rev. B*, **49**, 4866 (1994).
20. L. Daikhin and M. Urbakh, *Langmuir*, **12**, 6354 (1996).
21. M. Urbakh and L. Daikhin, *Langmuir*, **10**, 2836 (1994).
22. V. Tsionsky, G. Katz, E. Gileadi, and L. Daikhin, *J. Electroanal. Chem.*, **524-525**, 110 (2002).
23. L. Daikhin, E. Gileadi, G. Katz, V. Tsionsky, M. Urbakh, and D. Zagidulin, *Anal. Chem.*, **74**, 554 (2002).